PATTERN FORMATION IN ATHEROSCLEROTIC PLAQUES

by

Giuseppe Pasqualino

Submitted in partial fulfillment of the requirements
for the degree of Master of Science

at

Dalhousie University
Halifax, Nova Scotia
August 2019

To Tina my wife, nonna Teresa, and Elisa.

Table of Contents

List of Tables

List of Figures

Abstract

Atherosclerosis is a disease of the cardiovascular system that affects humans ubiquitously, and that can lead to myocardial infarction and stroke. It begins in the arterial blood vessel walls (intima) as an inflammatory response to dysfunction of the endothelium and access of the intima by oxidized low-density lipoproteins (oxLDLs). These phenomena trigger the recruitment of white blood cells, specifically monocytes, from the bloodstream. Trapped in the intima, the monocytes differentiate into macrophages which in turn, after engulfing the oxLDLs, become foam cells, leading to the production of inflammatory cytokines and further recruitment of white blood cells. This self-accelerating process results in a dramatic increase of the thickness of arteries, in the formation of atherosclerotic plaques and, possibly, in their rupture.

We suggest a one-dimensional mathematical model of the initiation and development of atherosclerosis which takes into account the concentration of immune cells and of pro- and anti-inflammatory cytokines. The model consists of a reaction–diffusion system with Neumann boundary conditions, and describes the recruitment of monocytes as a function of the concentration of inflammatory cytokines.

List of Abbreviations Used

IDL	high-density lipoprotein
IDL	intermediate-density lipoprotein
LDL	low-density lipoprotein
IL-8	interleukin-8
MCP-1	monocyte chemotactic protein 1
M-CSF	macrophage colony stimulating factor
ODE	ordinary differential equation
oxLDL	oxidized low-density lipoprotein
PDE	partial differential equation
PECAM-1	platelet endothelial cell adhesion molecule 1
SMC	smooth muscle cell
VLDL	very-low-density lipoprotein

Acknowledgements

I would like to thank my supervisor Dr. David Iron for sharing his knowledge, and for his patience and support of my Master's research and study, without which none of this work would have been possible. I would also like to thank Dr Darien L.J. DeWolf for his help and suggestions, and all the teachers and fellow students who graciously devoted some of their time to discussing Mathematics with me.

Chapter 1

Introduction

The use of mathematics as a tool for understanding biological and medical phenomena has increased significantly in the last few decades. One of the results of the interaction between mathematics and biology is the development of mathematical models to help and understand the structure, functioning, evolution, and diseases of the cardiovascular system.

Atherosclerosis (or atherosclerotic vascular disease) is one of the diseases that can affect this system. It consists of an anomalous condition affecting the wall of arterial vessels, characterized by the formation of deposits of fatty materials and the local formation of lesions called plaques in the wall of large arteries. Such plaques can form in the artery wall as early as infancy and continue to grow throughout adulthood, and may lead to significant narrowing of the artery lumen, which in turn can produce distal tissue ischaemia and thrombosis.

The early stages of atherosclerosis are non-symptomatic. Later on, depending on where the atherosclerotic plaque grows, symptoms may begin to occur, such as numbness or pain, and loss of function in certain parts of the body (examples include angina, peripheral arterial disease and kidney disease). Plaques may eventually become unstable and rupture, causing occlusions of the blood flow to vital organs, that may result in heart attack (acute myocardial infarction) and stroke (cerebrovascular accident), which are among the leading causes of death around the world.

1.1 Pathogenesis of Atherosclerosis

Atherosclerosis is a disease characterized by the accumulation of lipids, lipid-laden immune cells and cells that underwent apoptosis (i.e., programmed cell death) in the

arterial wall. The precursors of atherosclerotic lesions, the so-called fatty streaks, are observed in humans even during early childhood. Although the fatty streaks that can occur in infancy may be found throughout the arterial network, the advanced lesions of the disease of atherosclerosis are found in the larger arteries such as the abdominal aorta, coronary arteries, cerebral arteries and others [16].

A common site of lesions in the human artery is along the opposing wall of an arterial bifurcation, near branch points and along inner curvatures, where dynamical changes occur in the blood flow [33]. Contrary to the expectation that high shear stress could cause denudation of the arterial wall causing the damage that initiates the formation of atherosclerotic changes, a higher incidence of lesions has been observed at the sites of reduced shear stress. In 1969 and 1971, Caro, Fitz-Gerald and Schroter proposed that the mechanics of blood flow has a controlling rather than causative influence on atherogenesis. Caro et al. correlate the onset of arterial disease with a shear-dependent mass transfer mechanism and show that this is consistent with the observation of higher incidence of lesions at the sites of reduced shear stress [3].

The arteries where atherosclerosis develops, while of different sizes and locations in the body, have a similar structure. They can be thought of as tubes with a wall that contains three distinctive layers, whose innermost surface is exposed to flowing blood (see Figure 1.1).

The outermost layer, the adventitia, consists of fibroblasts, fibrocytes (collagen- and elastin-producing cells) and thick bundles of collagen fibres that provide reinforcement of the arterial wall.

The middle layer, the media, is the largest layer of the artery and consists of multiple layers of smooth muscle cells (SMCs) and an extracellular matrix of collagen and elastin. The muscular media is high in strength and is the most resistant layer to loads both in the axial and circumferential directions [14].

The intima is the innermost layer of the arterial wall. It is characterized by a mono-layer of endothelial cells that form the interface between the arterial wall and the blood flow, a thin basal membrane on which the endothelial cells rest and a

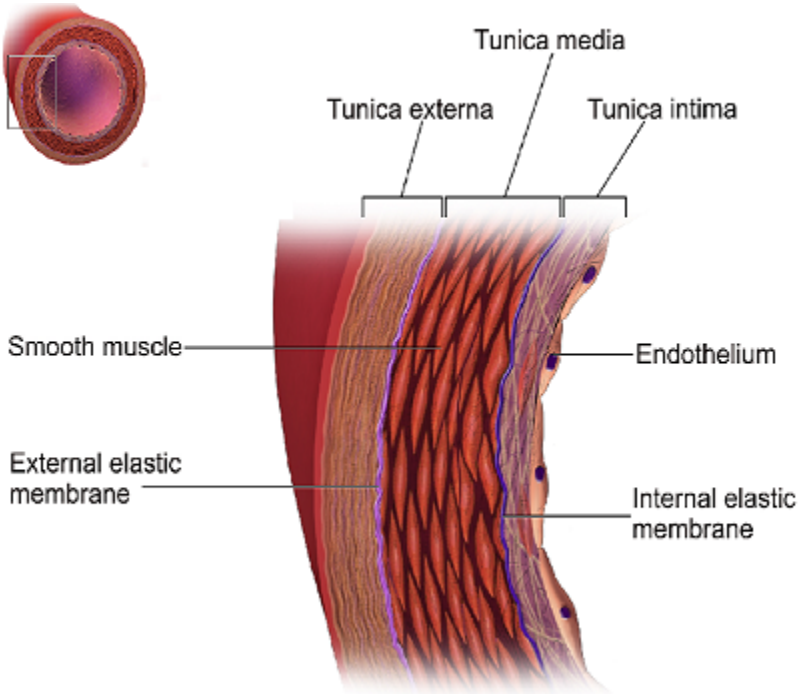

Figure 1.1: The layers of the human arterial wall. The figure shows—from right to left—the intima composed of the monolayer of endothelial cells, and a subendothelial layer containing proteoglycans and collagen fibrils resting on an internal elastic lamina. Further into the wall is the media composed primarily of layered SMCs. The external layer, the adventitia, contains fibroblasts, fibrocytes, and collagen fibres. [34]

subendothelial layer of SMCs, proteoglycans (complex molecules with a protein core and particular types of sugar, called glycosaminoglycans, attached) and collagen fibrils (fibrous protein complexes). The inflammation that characterizes the atherogenic process takes place primarily within this layer. The endothelial cells serve several purposes that include providing a smooth surface for fluid flow, secretion of anticoagulants to maintain the fluid state of the blood and chemical signaling of immune cells. This barrier assumes great significance in the development of and protection against atherosclerosis by regulating the passage of chemical and cellular species between the artery wall and the adjacent bloodstream, via increasing or decreasing the expression of adhesion molecules.

The theory that atherosclerosis is a chronic inflammatory response to injury is now accepted as a general concept among researchers in the field [28].

The first step of the disease involves endothelial dysfunction. Although poorly

understood, this process appears to be characterized by a change in the permeability of the endothelial layer that allows lipids to migrate into the subendothelial layer followed by an influx of immune cells. The change in permeability is also accompanied by an increase in the adhesiveness of the endothelial layer (expression of adhesion molecules on the surface of the endothelium triggered by the presence of modified low-density lipoproteins (LDL) [12], and a change from anticoagulant to procoagulant properties [24, 23]. A number of factors have been considered as possible causes of endothelial dysfunction. These include cigarette smoking, diabetes mellitus and hypertension (all of which generate free radicals which activate LDL oxidation), elevated LDL cholesterol blood levels and possibly even infection by microorganisms (e.g., herpes viruses or Chlamydia Pneumoniae) [29] (Figure 1.2).

Following endothelial dysfunction and migration of lipoproteins and immune cell, we identify steps in disease progression. These are chemical modification of LDL, corruption of the immune response, and lesion growth.

1.1.1 Chemical Modification of LDL. Corruption of the Immune Response.

Lipoproteins are micellar particles produced by the liver and intestines which contain regulatory proteins that direct the blood trafficking of cholesterol and other lipids to various cells in the body. There are four major classes of lipoprotein: very low-density lipoprotein (VLDL), intermediate-density lipoprotein (IDL), low-density lipoprotein (LDL) and high-density lipoprotein (HDL). The lipoprotein structure consists of a lipid core containing cholesterol esters and triglycerides, and a coat that is composed of regulatory surface proteins, unesterified cholesterol, phospholipids and a variety of other components that may include molecules associated with antioxidant defences. LDL particles transport cholesterol that is needed for various cellular functions such as cell membrane formation and hormone synthesis. Although LDL particles are not found in atherosclerotic plaques, oxidatively modified LDL particles are.

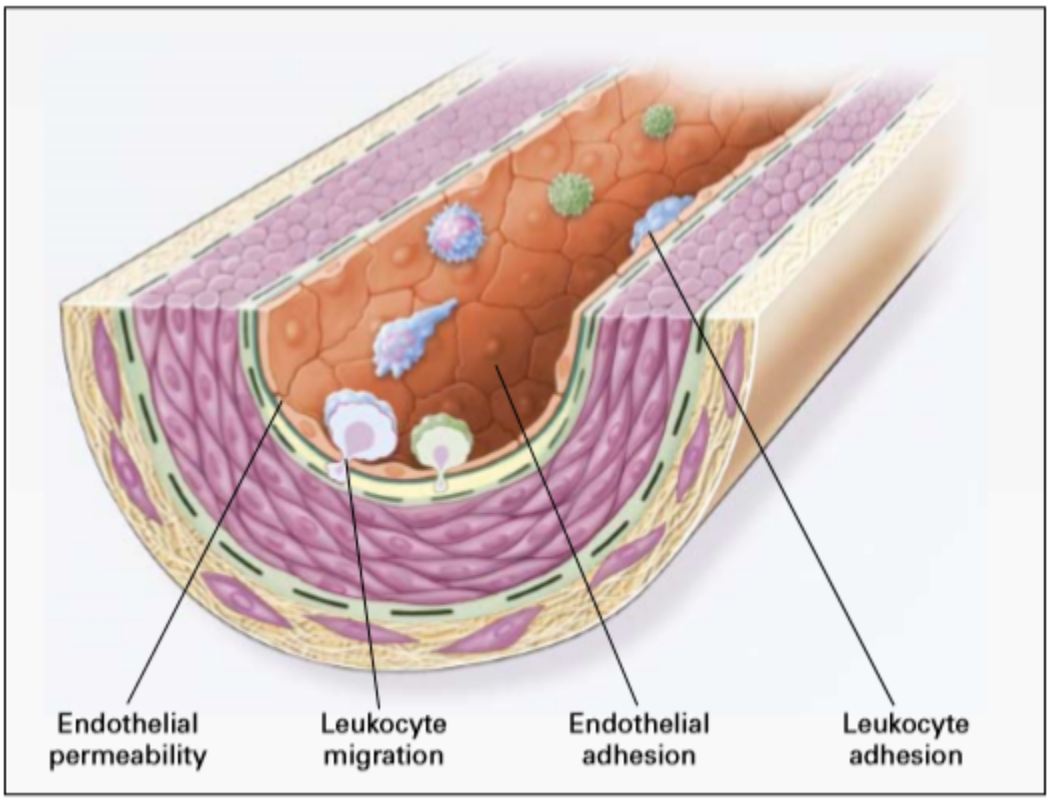

Figure 1.2: Endothelial Dysfunction in Atherosclerosis. The earliest changes that precede the formation of lesions of atherosclerosis take place in the endothelium. These changes include increased endothelial permeability to lipoproteins and other plasma constituents, which is mediated by nitric oxide, prostacyclin, platelet-derived growth factor, angiotensin II, and endothelin; up-regulation of leukocyte adhesion molecules, including L-selectin, integrins, and platelet–endothelial-cell adhesion molecule 1, and the up-regulation of endothelial adhesion molecules, which include E-selectin, P-selectin, intercellular adhesion molecule 1, and vascular-cell adhesion molecule 1; and migration of leukocytes into the artery wall, which is mediated by oxidized low-density lipoprotein, monocyte chemotactic protein 1, interleukin-8, platelet-derived growth factor, macrophage colony-stimulating factor, and osteopontin. Reproduced with permission from [29], Copyright Massachusetts Medical Society.

As described above, the LDL particle contains on its surface a number of antioxidant defenses including α-tocopherol (vitamin E). In the plasma, where the concentration of free radicals is low and other antioxidant particles are present, LDL usually remains in its native, unoxidized form. Following the changes in the permeability of the endothelial layer and the up-regulation of receptors for LDL by endothelial cells [29], the LDL particle is transported into the intima, and it may expend all of its innate defenses against oxidation. Once LDL is oxidized, it is recognized by the scavenger receptor on the surface of the macrophages. Exacerbating the problem is the fact that oxLDL particles are trapped in the artery wall [5]. Attracted by oxLDL, the macrophages in the artery wall attempt to internalize the lipoprotein particles. This results in an accumulation of lipids -cholesterol esters- and transformation of the macrophage into a foam cell. In this lipid-laden state, the macrophage is incapable of functioning normally. As a result, dead or apoptotic cells and other debris (including the foam cells) are allowed to build up. In response, chemoattractants (chemical signals) including monocyte chemotactic protein 1 (MCP-1), interleukin-8 (IL-8) and macrophage colony-stimulating factor(M-CSF) are secreted by the foam cells and endothelial cells to summon more immune cells to the site. Circulating immune cells in the blood, such as monocytes and T-lymphocytes, migrate into the subendothelial layer in response to the chemical signals. Once in the artery wall, monocytes differentiate into macrophages in response to macrophage colony stimulating factor (M-CSF) [24, 29]. These macrophages begin to exhibit scavenger receptors on their surface [12]. The chemical mediators of inflammation can increase binding of oxLDL to cells in the arterial wall. Hence, the new macrophages become engorged with oxLDL and the cycle of chemical signaling continues, instigating plaque growth.

Moreover, a source of additional immune cells include migration via the vasa vasorum, the vascular network that perfuses the arterial wall with blood.

This auto-amplification phenomenon is compensated by an anti-inflammatory phenomenon mediated by the anti-inflammatory cytokines which inhibit the production of pro-inflammatory cytokines (biochemical anti-inflammation) (Figure 1.3).

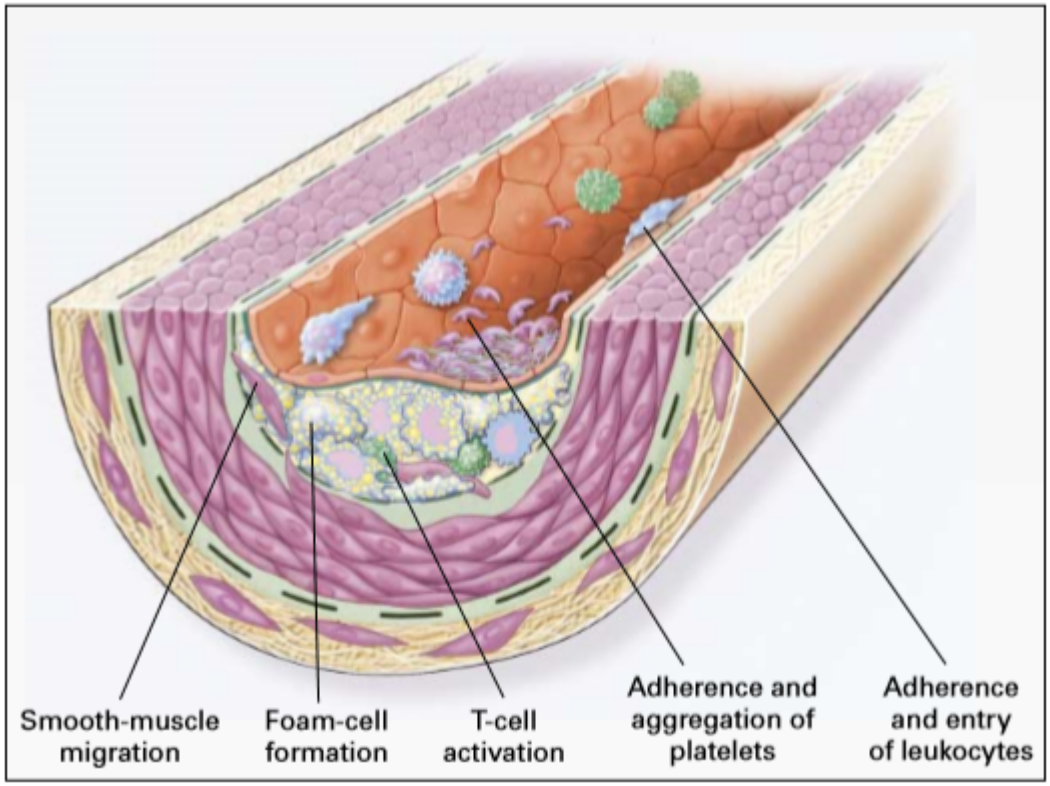

Figure 1.3: Fatty-Streak Formation in Atherosclerosis. Fatty streaks initially consist of lipid-laden monocytes and macrophages (foam cells) together with T lymphocytes. Later they are joined by various numbers of smooth-muscle cells. The steps involved in this process include smooth-muscle migration, which is stimulated by platelet-derived growth factor, fibroblast growth factor 2, and transforming growth factor β; T-cell activation, which is mediated by tumor necrosis factor α, interleukin-2, and granulocyte–macrophage colony-stimulating factor; foamcell formation, which is mediated by oxidized low-density lipoprotein, macrophage colony-stimulating factor, tumor necrosis factor α, and interleukin-1; and platelet adherence and aggregation, which are stimulated by integrins, P-selectin, fibrin, thromboxane A_2, tissue factor, and the factors described in Figure 1 as responsible for the adherence and migration of leukocytes. Reproduced with permission from [29], Copyright Massachusetts Medical Society.

1.1.2 Lesion Growth

SMCs also respond to chemical signals produced during the accumulation of oxLDL, foam cells and debris. SMCs migrate around the lesion to form a fibro-muscular cap overlaying the plaque. This process is also mediated by chemoattractants which entice SMCs into the region as well as chemoinhibitors that keep the SMCs outside of the lesion core [25]. The cap of SMCs and poorly formed connective tissue covers the core which contains dead cells, foam cells and potentially necrotic tissue. Eventually, there is encroachment of the arterial lumen as the cells, cell matrix and debris accumulate in the plaque. The overlaying surface becomes thrombogenic resulting in platelet adherence due to increase in expression of platelet–endothelial cell adhesion molecule 1 (PECAM-1). The thrombus can further diminish or even completely occlude blood flow at this site [29]. Continued disease progression results in an advanced lesion described as a fibrous plaque. These types of plaques are characterized by a dense cap composed of SMCs, collagen, elastin and basement membrane fibres. These plaques often cause various degrees of arterial occlusion. However, the danger of clinically significant ischemia imposed by such a lesion has more to do with the stability of the plaque (which is primarily determined by the composition of the cap and the lipid core) than the degree of occlusion caused by the plaque [6, 9]. A non-uniform cap with a region that is thin (commonly found at the 'shoulders' of the plaque) is mechanically unstable. Rupture of an unstable but moderate-sized plaque can result in complete occlusion of an artery with catastrophic medical consequences such as stroke or myocardial infarction. Whereas a lesion that may occlude the lumen to a much greater extent but which has a stable cap may be less of an immediate threat to a person because neovascular development can compensate for the chronic and slowly forming occlusion. (Figure 1.4)

The disease of atherosclerosis, and its initiation atherogenesis, involves a complex interplay between mechanical, genetic, pathogenic, and biochemical processes. Although a comprehensive view of atherosclerosis will ultimately require integration

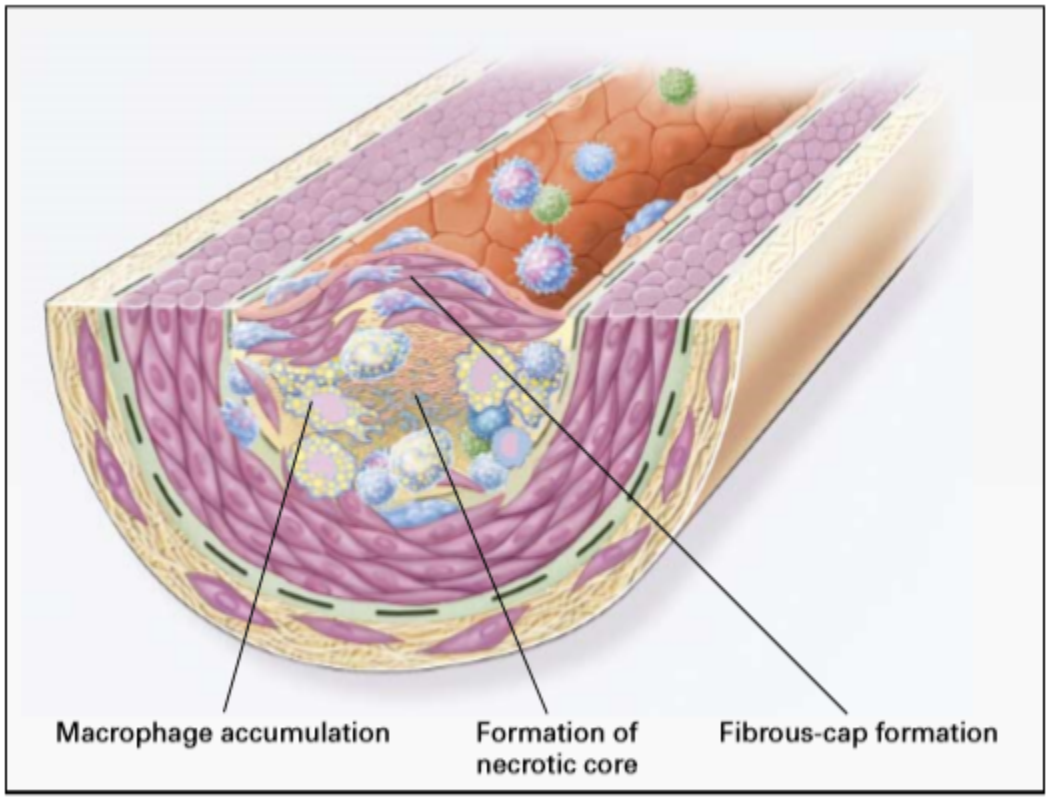

Figure 1.4: Formation of an Advanced, Complicated Lesion of Atherosclerosis. As fatty streaks progress to intermediate and advanced lesions, they tend to form a fibrous cap that walls off the lesion from the lumen. This represents a type of healing or fibrous response to the injury. The fibrous cap covers a mixture of leukocytes, lipid, and debris, which may form a necrotic core. These lesions expand at their shoulders by means of continued leukocyte adhesion and entry caused by the same factors as those listed in Figures 1 and 2. The principal factors associated with macrophage accumulation include macrophage colony-stimulating factor, monocyte chemotactic protein 1, and oxidized low-density lipoprotein. The necrotic core represents the results of apoptosis and necrosis, increased proteolytic activity, and lipid accumulation. The fibrous cap forms as a result of increased activity of platelet-derived growth factor, transforming growth factor β, interleukin-1, tumor necrosis factor α, and osteopontin and of decreased connective-tissue degradation. Reproduced with permission from [29], Copyright Massachusetts Medical Society.

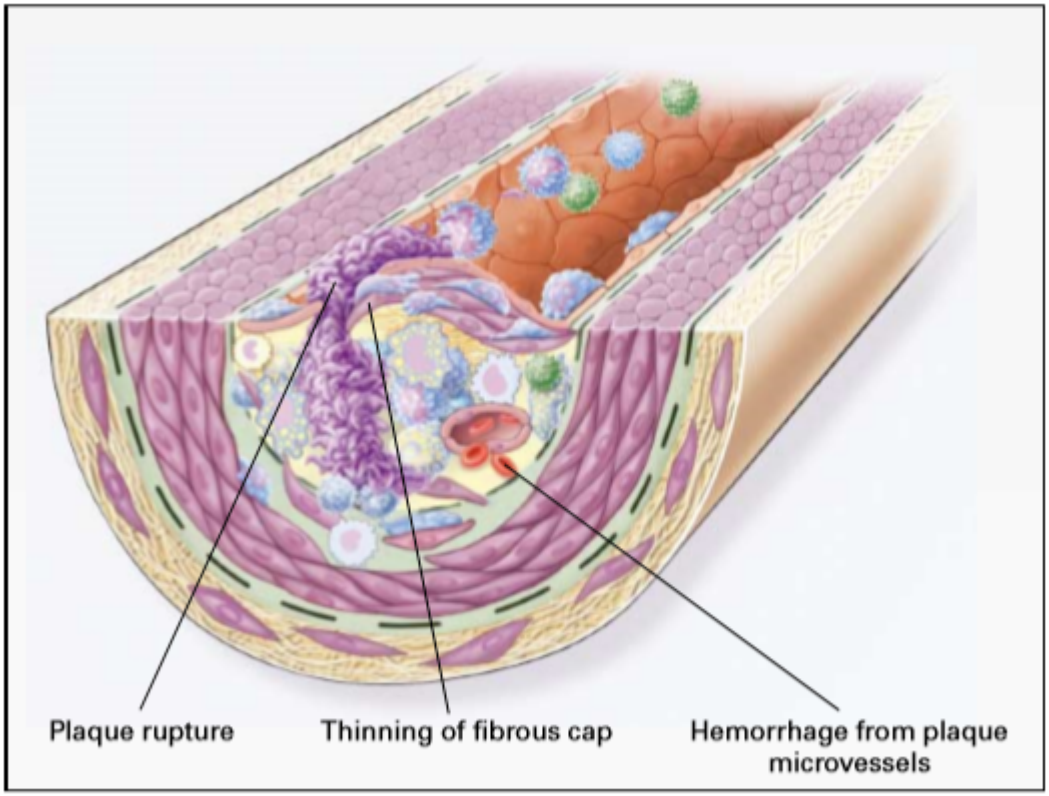

Figure 1.5: Unstable Fibrous Plaques in Atherosclerosis. Rupture of the fibrous cap or ulceration of the fibrous plaque can rapidly lead to thrombosis and usually occurs at sites of thinning of the fibrous cap that covers the advanced lesion. Thinning of the fibrous cap is apparently due to the continuing influx and activation of macrophages, which release metalloproteinases and other proteolytic enzymes at these sites. These enzymes cause degradation of the matrix, which can lead to hemorrhage from the vasa vasorum or from the lumen of the artery and can result in thrombus formation and occlusion of the artery. Reproduced with permission from [29], Copyright Massachusetts Medical Society.

of these various modeling perspectives, building a model that takes into account all the aspects of this process, even with all the necessary simplifications, would be a titanic and daunting endeavour. Instead, researchers have been focusing on models that study particular aspects.

Some fluid dynamical models consider the interaction between blood flow and vessel walls [31, 32], or study the coupling of the haemodynamics and mass transfer with a simple lesion growth in the intima.

Mathematical approaches have been used to study lipoprotein transport and accumulation in the arterial wall [26, 30], and in vitro LDL oxidation [5].

Other types of mathematical models, such as that of the present work, have been devised to study the role of the biochemical processes in the formation of plaques. They are based on partial or ordinary differential equations, describing the reactions between immune cells (primarily macrophages), smooth muscle cells, chemoattractant and low-density lipoproteins, see for instance [4, 8, 17].

El Khatib et al. have proposed one and two-dimensional reaction–diffusion models to describe the response in the intima of the artery vessel [8]. Related works are Cobbold et al.[5], Li et al.[21], Ougrinovskaia et al.[27]; El Khatib et al.[7]; Hidalgo et al.[13].

In this paper we propose a mathematical model that describes the early stages of atherosclerosis, focusing on the inflammatory component of atherogenesis. In particular, we model the secretion of and the response to chemotactic stimuli by various immune-cell species and LDL, and the behaviour of immune cells – primarily macrophages – in the presence of oxidatively modified LDL and cytokines, in the blood and arterial wall. Our model incorporates many parameters characterizing such things as the rate at which macrophages move within the intimal tissue in response to chemokine (chemoattractants, cytokines), degradation rates of various chemicals, chemical reaction rates and so forth.

Because this study centres on the interplay between chemical and cellular species in the human arteries and bloodstream, we employ a classical model of chemotaxis

(which is the phenomenon of micro-organisms or cells "sensing" chemical gradients and moving in response to them) first presented by E. F. Keller and Lee Segel in their seminal 1970 work [19]. The original model consists of two partial differential equations (PDEs) which couple together the density of amoebae and the concentration of the chemo-attractant. Keller-Segel system and its variants have been used in a wide variety of contexts. It is one of the simplest systems of PDE models that has very intricate solution structure but that is still accessible to a wide range of mathematical techniques, including the study of existence/uniqueness of solutions, blowup analysis, and pattern formation. For an extensive review see [15] and references therein.

The purpose of this paper is to study basic pattern formation in a model of chemotaxis with self-production terms. To this end we will analyze a coupled system of non-linear reaction diffusion equations describing the state of the various species involved in the disease process.

This approach is inspired by the study by Kolokolnikov et al. [20]

In chapter 2 we lay out the assumptions upon which the mathematical model is constructed. This is followed by a presentation and an analysis of the general model. In chapter 3 we discuss our results.

The computations in this paper were performed by using Maple™. The numerical simulations in this paper were performed by using FlexPDE solver (FlexPDE6 PDE Solutions Inc., URL www.pdesolutions.com)

Chapter 2

The Model

In constructing our model we had to adopt by necessity a simplified view of a complicated process.

Our work is based on a continuum mechanical view of the process of formation of an atherosclerotic plaque. Hence, the equations governing the dynamics of various species involved are derived by considering a balance of mass of each species. To this end, we identify the cellular and chemical species most significant to the process and consider their production, movement, and death in an arbitrary region. In so doing, we account for the highly interactive nature of disease development, the secretion of chemical species by cells, movement of cells in response to chemical signals and so forth.

2.1 Modelling Assumptions

Based on the literature we identify the following four cellular and chemical species that are to be considered responsible for disease described in this model:

I: A density measurement for immune cells (g/mm^3). These are primarily monocyte-derived macrophages but may also include monocytes, T-lymphocytes and other immune response cells.

F: A density measurement for foam Cells (g/mm^3). These are modified macrophages.

C: A concentration measurement for chemoattractant (e.g., µmol/l). Here, we make no distinction between various types of chemoattractants, such as macrophage colony-stimulating factor, monocyte chemotactic protein, interleukin-1 and others. Rather, C refers to any chemical that induces positive chemotaxis (i.e., in the direction of higher concentration of the chemoattractant).

L: A concentration measurement for OxLDL (oxidized LDL molecules)(mmol/l).

The change in the concentration of each species is subject to the following assumed conditions:

1. Endothelial dysfunction occurs by an unspecified mechanism allowing LDL to enter the intima.

2. Immune cells exhibit positive chemotaxis in response to chemoattractant and oxLDL. Cells are sensitive to the relative concentration gradient with respect to taxis. This is consistent with the observation that cells are highly sensitive to changes in chemical concentration at very low concentrations, and it also accounts for saturation effects at high concentrations.

3. Chemoattractant is produced by cells in the arterial intima (immune cells, endothelial cells, etc.), and is removed in an unspecified way (i.e., by a combination of the following mechanisms: neutralization on contact by immune cell or SMC, inhibition by the anti-inflammatory cytokines, or because of its kinetics).

4. Immune cells die or become corrupted to produce debris.

5. The concentration of foam cells increases due to corruption of macrophages, and it decreases by degradation by immune cells in the course of normal immune function.

6. All species are subject to some random flux through the boundary of a volume.

2.2 Model Equations

In our model, we first considered a one-dimensional reaction-diffusion system of four PDEs on an interval representing the arterial intima:

$$
\begin{aligned}
L_t &= D_L L_{xx} + \frac{\alpha_L}{L+\beta} - \mu_L L - K_L LI \\
C_t &= D_c C_{xx} + K_F F + K_I I - \mu_C C \\
F_t &= \epsilon^2 F_{xx} + K_L LI - \mu_F F \\
I_t &= D_I I_{xx} + \frac{\alpha_I}{I+\beta} - \mu_I I - K_L LI - \chi \left(\frac{I}{C} C_x \right)_x
\end{aligned}
$$

Successive numerical simulations have suggested that the pattern formation involved in the building of an atherosclerotic plaque is driven by the change in the concentrations of immune cells and chemo-attractant. So, for the sake of clarity, we will analyze the simplest reasonable model:

$$
\begin{aligned}
I_t &= D_I I_{xx} + \frac{\alpha_I}{I+\beta_I} - \mu_I I - \chi (I C_x)_x \\
C_t &= D_c C_{xx} + K_I I - \mu_C C,
\end{aligned}
\tag{2.1}
$$

coupled with Neumann boundary conditions

$$
I_x(\pm L, t) = 0 = C_x(\pm L, t). \tag{2.2}
$$

In the first equation of Equation (2.1), the term $D_I I_{xx}$ describes the diffusion of the immune cells from the arterial blood to the arterial wall, and D_I represents the diffusion coefficient of the immune cells. The term $\frac{\alpha_I}{I+\beta_I}$ describes the production of immune cells, α_I represents the production rate of immune cells, and β_I represents the negative feedback on production of the immune cells, which, for the purpose of this study, is caused by unspecified anti-inflammatory chemical species (notice that the added constant β_I in the denominator guarantees that this quantity doesn't grow without bound). The term $\mu_I I$ describes the decay of immune cells; here μ_I is the decay rate of the immune cells. The term $\chi(IC_x)_x$ describes the chemotaxis of immune cells from the blood into the intima, promoted by the inflammatory cytokines. This term models the sensing mechanism and cells diffuse with diffusion coefficient D_I. The factor χ represents the strength of the chemoattractant.

In the second equation of Equation (2.1), the term $D_c C_{xx}$ describes the diffusion of chemo-attractant to the arterial blood, and D_C represents the diffusion coefficient of the chemoattractant. The term $K_I I$ describes the production of chemo-attractant by the immune cells, here K_I represents the production rate of chemoattractant by immune cells. The term $\mu_C C$ describes the decay of chemo-attractant; the factor μ_C represents the decay rate of the chemoattractant.

The homogeneous Neumann conditions imposed on the concentration of immune cells I and on the concentration of chemoattractant C represent the inability of these species to pass through the respective boundaries. That is, we assume that the velocity of fluid flow in the axial direction is sufficiently large to result in a near-zero flux of immune cells and chemoattractant into or out of the region of interest (from the lumen).

2.3 The Scaled Model

Since it was first presented in 1970, the Keller-Segel model of chemotaxis has been studied extensively [15], and it is well known that it generates spike-type solutions, which correspond to small localized regions of high concentration of the quantities under study (in our case immune cells and chemoattractant cytokines), with relatively small concentrations of them elsewhere.

Numerical simulations suggest that the height of a spike solution to our system is $O\left(\frac{1}{\epsilon}\right)$. It is of practical benefit (for instance, to simplify numerical simulations) to scale Equations (2.1) by applying the following transformations, after dropping the *'s :

$$I = \frac{1}{\epsilon} I^*, \quad C = \frac{1}{\chi} C^*, \quad D_I = \epsilon.$$

Here $\epsilon << 1$, because in our model we assume that the immune cells do not have a great deal of movement.

So, we obtain the following equations:

$$\begin{aligned} I_t &= \epsilon I_{xx} - (IC_x)_x + \epsilon^2 \frac{\alpha_I}{I + \epsilon\beta_I} - \mu_I I, \\ C_t &= D_c C_{xx} + \frac{\chi K_I I}{\epsilon} - \mu_C C. \end{aligned} \tag{2.3}$$

We will first construct a solution consisting of a single spike for I which is centered at the origin, $x = 0$, and has a width $O(\epsilon)$. We will call this region centered at the origin *inner region*, and we will call any x in this interval an *inner variable*. We will call the region where $|x| > O(\epsilon)$ *outer region*, and we will call any x in this interval an *outer variable*.

We investigate two theoretically possible solutions for the system in Equation (2.3); following the example of Kolokolnikov et al. [20], we will call them Type 1 solution and Type 2 solution, respectively.

Type 1 solution is characterized by strict localization of I to the inner region. We will show that such solution cannot exist. Nonetheless it does make sense to consider local Type 1 solution, since it will be one of the two terms that constitute Type 2 solution. We study Type 1 solution in Section 2.3.1. Type 2 solution, which we study in Section 2.3.2, is a feasible solution of our system; it is also more complicated, and, in the outer region, it satisfies a nonlinear third order ordinary differential equation (ODE).

We note here that the values used to perform the numerical simulations were assigned ad hoc so that the initial assumptions would be qualitatively satisfied. The attainment of biologically precise parameter values can be very difficult especially with respect to in vivo studies. The values we used were chosen to highlight the impact of the various parameters. We expected this simpler system would capture two primary features of the disease process, namely localization and aggregation.

The parameter values used in all calculations are given in the table below:

2.3.1 Type 1 Solution

We begin the analysis of our simplified system by considering the steady state of Equations (2.3). We will then proceed to construct a symmetric spike centered at

Table 1 Parameter Values			
ϵ	0.1	D_C	4
α_I	0.75	K_I	1.95
β_I	1	χ	14
μ_I	1	μ_C	4

Table 2.1: Parameter Values

the origin. This is equivalent to constructing a half-spike on the interval $[0, L]$, with Neumann boundary conditions for I and C at $x = 0, L$.

At the steady state the equations on the half domain $x \in [0, L]$ are:

$$\begin{aligned} \epsilon I_{xx} - (IC_x)_x + \frac{\epsilon^2 \alpha_I}{I + \epsilon\beta_I} - \mu_I I = 0 \\ D_c C_{xx} + \frac{\chi K_I I}{\epsilon} - \mu_C C = 0, \end{aligned} \tag{2.4}$$

with Neumann boundary conditions

$$I_x(0,t) = I_x(L,t) = C_x(0,t) = C_x(L,t) = 0.$$

The analysis of this system is similar to that in [20].

To study the behavior of the solutions of our system of differential equations in the inner region we introduce the following change of the inner variable:

$$\begin{aligned} x &= \epsilon y \\ I &= \tilde{I}(y) \\ C &= C_0 + \epsilon \widetilde{C}(y) \end{aligned}$$

where $C_0 = C(0)$ is to be determined, and $\widetilde{C}(0)$=0.

Notice that the scaling of x, which will benefit us in our calculations, is equivalent to zooming in on the interval $(-\epsilon, \epsilon)$ around the origin.

Then, we can perform the following changes:

$$\epsilon I_{xx} \to \frac{1}{\epsilon}\tilde{I}_{yy}$$
$$(IC_x)_x = I_x C_x + IC_{xx} \to \frac{1}{\epsilon}(\tilde{I}_y \widetilde{C}_y + \tilde{I}\widetilde{C}_{yy}) = \frac{1}{\epsilon}(\tilde{I}\widetilde{C}_y)_y$$
$$D_c C_{xx} \to \frac{D_c}{\epsilon}\widetilde{C}_{yy}$$

So we obtain the following problem in the inner variable:

$$\frac{1}{\epsilon}\tilde{I}_{yy} - \frac{1}{\epsilon}(\tilde{I}\widetilde{C}_y)_y + \epsilon^2 \frac{\alpha_I}{\tilde{I} + \epsilon\beta_I} - \mu_I \tilde{I} = 0$$
$$\frac{D_c}{\epsilon}\widetilde{C}_{yy} + \frac{\chi K_I \tilde{I}}{\epsilon} - \mu_C(\epsilon\widetilde{C} + C_0) = 0$$

or

$$\begin{aligned} \tilde{I}_{yy} - (\tilde{I}\widetilde{C}_y)_y + \epsilon^3 \frac{\alpha_I}{\tilde{I} + \epsilon\beta_I} - \epsilon\mu_I \tilde{I} = 0 \\ D_c\widetilde{C}_{yy} + \chi K_I \tilde{I} - \epsilon\mu_C(\epsilon\widetilde{C} + C_0) = 0. \end{aligned} \tag{2.5}$$

with the Neumann Boundary Conditions

$$\tilde{I}_{0y}(0,t) = \tilde{I}_{0y}(\infty,t) = \widetilde{C}_{0y}(0,t) = \widetilde{C}_{0y}(\infty,t) = 0.$$

By means of ϵ-power series expansion, we can write the functions $\tilde{I}$ and $\widetilde{C}$ as

$$\tilde{I} = \tilde{I}_0 + \epsilon\tilde{I}_1 + ...$$
$$\widetilde{C} = \widetilde{C}_0 + \epsilon\widetilde{C}_1 + ...$$

We substitute these expressions in Equation (2.5). To leading order, considering $\epsilon << 1$, we obtain the system

$$\begin{aligned} \tilde{I}_{0yy} - \left(\tilde{I}_0\widetilde{C}_{0y}\right)_y = 0 \\ D_c\widetilde{C}_{yy} + \chi K_I \tilde{I}_0 = 0. \end{aligned} \tag{2.6}$$

with the Neumann boundary conditions

$$\tilde{I}_{0y}(0,t) = \tilde{I}_{0y}(\infty,t) = \widetilde{C}_{0y}(0,t) = \widetilde{C}_{0y}(\infty,t) = 0.$$

From the first equation in Equation (2.6) we can see that $\tilde{I}_{0y} - \tilde{I}_0\widetilde{C}_{0y} = c$, for some constant c.

Since $\tilde{I}_{0y} \to 0$ and $\widetilde{C}_{0y} \to 0$ as $y \to 0$ (because of the Neumann boundary conditions), we have that $c = 0$.

So we obtain the following:

$$\widetilde{C}_{0y} = \frac{\tilde{I}_{0y}}{\tilde{I}_0} \tag{2.7}$$

and

$$D_c\widetilde{C}_{yy} + \chi K_I\tilde{I}_0 = D_c(\frac{\tilde{I}_{0y}}{\tilde{I}_0})_y + \chi K_I\tilde{I}_0 = 0. \tag{2.8}$$

Thus

$$\left(\frac{\tilde{I}_{0y}}{\tilde{I}_0}\right)_y + \frac{\chi K_I}{D_c}\tilde{I}_0 = 0. \tag{2.9}$$

Let $u = \log(\tilde{I}_0)$ and $\tilde{I}_0 = e^u$.

Differentiating these expressions we obtain

$$u_y = \frac{\tilde{I}_{0y}}{\tilde{I}_0} \qquad \text{and} \qquad u_{yy} = \left(\frac{\tilde{I}_{0y}}{\tilde{I}_0}\right)_y.$$

Substituting these in Equation (2.8) we have

$$u_{yy} + \frac{\chi K_I}{D_c}e^u = 0.$$

Multiplying both sides by u_y we get

$$u_{yy}u_y + \frac{\chi K_I}{D_c}e^u u_y = 0,$$

or

$$\frac{d}{dy}\left[\frac{1}{2}(u_y)^2 + \frac{\chi K_I}{D_c}e^u\right] = 0.$$

Therefore we have

$$\frac{1}{2}(u_y)^2 + \frac{\chi K_I}{D_c}e^u = c_1, \tag{2.10}$$

where c_1 is a constant.

At $x = 0$ we have that $\tilde{I}_0(0) = \xi$ (where ξ is to be determined) and $\tilde{I}_{0y}(0) = 0$, because of the Neumann boundary conditions.

So $u(0) = \log(\xi)$ and $u_y(0) = 0$.

Hence Equation (2.10) becomes

$$\frac{\chi K_I}{D_c}e^{\log(\xi)} = c_1.$$

Thus, we see that

$$c_1 = \frac{\chi K_I}{D_c}\xi.$$

Substituting c_1 in Equation (2.10) we get

$$\frac{1}{2}(u_y)^2 + \frac{\chi K_I}{D_c}e^u = \frac{\chi K_I}{D_c}\xi,$$

or

$$(u_y)^2 = 2\frac{\chi K_I}{D_c}(\xi - e^u).$$

Therefore we have that

$$u_y = \pm\sqrt{2\frac{\chi K_I}{D_c}(\xi - e^u)}.$$

Here we consider only the negative solutions since u is a decreasing function. Now we may integrate the expression $\frac{du}{dy} = -\sqrt{2\frac{\chi K_I}{D_c}(\xi - e^u)}$ to obtain

$$\int -\frac{du}{\sqrt{2\frac{\chi K_I}{D_c}(\xi - e^u)}} = \int dy,$$

$$-\frac{1}{\sqrt{2\frac{\chi K_I}{D_c}}}\int \frac{du}{\sqrt{\xi - e^u}} = y + c_2,$$

$$-\frac{1}{\sqrt{2\frac{\chi K_I}{D_c}}}\frac{\log\left(\frac{|\sqrt{\xi-e^u}-\sqrt{\xi}|}{\sqrt{\xi-e^u}+\sqrt{\xi}}\right)}{\sqrt{\xi}} = y + c_2,$$

$$\frac{2}{\sqrt{2\frac{\chi K_I}{D_c}}}\frac{\tanh^{-1}\left(\frac{\sqrt{\xi-e^u}}{\sqrt{\xi}}\right)}{\sqrt{\xi}} = y + c_2,$$

$$\tanh^{-1}\left(\frac{\sqrt{\xi - e^u}}{\sqrt{\xi}}\right) = (y + c_2)\sqrt{\frac{\xi\chi K_I}{2D_c}}.$$

So

$$\frac{\sqrt{\xi - e^u}}{\sqrt{\xi}} = \tanh\left[(y + c_2)\sqrt{\frac{\xi\chi K_I}{2D_c}}\right].$$

Thus

$$\xi - e^u = \xi\tanh^2\left[(y + c_2)\sqrt{\frac{\xi\chi K_I}{2D_c}}\right].$$

Therefore

$$\tilde{I}_0 = e^u = \xi\left\{1 - \tanh^2\left[(y + c_2)\sqrt{\frac{\xi\chi K_I}{2D_c}}\right]\right\} = \xi\,\mathrm{sech}^2\left[(y + c_2)\sqrt{\frac{\xi\chi K_I}{2D_c}}\right].$$

Differentiating this expression, we get

$$\tilde{I}_{0y} = -\xi\sqrt{\frac{\xi\chi K_I}{2D_c}}\,\mathrm{sech}^2\left[(y + c_2)\sqrt{\frac{\xi\chi K_I}{2D_c}}\right]\tanh\left[(y + c_2)\sqrt{\frac{\xi\chi K_I}{2D_c}}\right]. \tag{2.11}$$

Since $\tilde{I}_{0y}(0) = 0$, due to the boundary conditions, and because

$$-\sqrt{\frac{\xi\chi K_I}{2D_c}}\,\mathrm{sech}^2\left[(c)\sqrt{\frac{\xi\chi K_I}{2D_c}}\right] \neq 0$$

for all values of c_2, in order for the right-hand side of equation (2.11) to be 0 at $y = 0$, we must have that $\tanh\left[(y+c)\sqrt{\frac{\xi\chi K_I}{2D_c}}\right] = 0$.

Since $\frac{\chi K_I}{D_c} \neq 0$, we see that $c_2 = 0$.

Then

$$\tilde{I}_0 = \xi \operatorname{sech}^2\left(y\sqrt{\frac{\xi\chi K_I}{2D_c}}\right),$$

where ξ, the height of the spike, is the free parameter that is due to the scaling invariance of the problem in Equation (2.4). We will solve for ξ by matching the inner and outer solutions.

Substituting the expression for $\tilde{I}_0$ in Equation (2.7), we can also find an expression for $\widetilde{C}_{0y}$:

$$\begin{aligned}\widetilde{C}_{0y} = \frac{\tilde{I}_{0y}}{\tilde{I}_0} &= \frac{-\xi\sqrt{\frac{2\xi\chi K_I}{2D_c}}\operatorname{sech}^2\left(y\sqrt{\frac{\xi\chi K_I}{2D_c}}\right)\tanh\left(y\sqrt{\frac{\xi\chi K_I}{2D_c}}\right)}{\xi\operatorname{sech}^2\left(y\sqrt{\frac{\xi\chi K_I}{2D_c}}\right)} \\ &= -\xi\sqrt{\frac{2\xi\chi K_I}{2D_c}}\tanh\left(y\sqrt{\frac{\xi\chi K_I}{2D_c}}\right).\end{aligned}$$

Summarizing, in the inner region we have the solution

$$\begin{aligned}\tilde{I}_0 &= \xi\operatorname{sech}^2\left(y\sqrt{\frac{\xi\chi K_I}{2D_C}}\right) \\ \widetilde{C}_{0y} &= -\sqrt{\frac{2\xi\chi K_I}{D_C}}\tanh\left(y\sqrt{\frac{\xi\chi K_I}{2D_C}}\right).\end{aligned} \tag{2.12}$$

To determine the height ξ of the spike, we now consider the outer region

$|x| >> \epsilon$.

First, we shall find a function C that solves the second equation in (2.6) away from the center of the spike. We will then use it to find a global solution on the entire interval which, in turn, will be instrumental in finding ξ.

To this end, we notice that in the outer region $I \sim 0$. Then from the second equation in Equation (2.4) we have

$$D_c C_{xx} - \mu_c C = -\frac{\chi K_I}{\epsilon} I \sim 0.$$

Let us consider the right hand side of this equation. We notice that the quantity $\frac{I}{\epsilon}$ behaves like a rectangular pulse of width ϵ and height $\frac{1}{\epsilon}$. In the limit as $\epsilon \to 0$, this approaches an infinitely concentrated pulse $\delta(x-x_0)$, which would be zero everywhere except at $x = 0$, where it would be ∞.

Thus, we can treat $-\frac{\chi K_I}{\epsilon} I$ as a multiple of the δ-function, that is

$$\frac{\chi K_I}{\epsilon} I(x) = \beta\delta(x - x_0).$$

So C in the outer region satisfies the problem

$$D_c C''(x) - \mu_c C(x) = -\beta\delta(x - x_0)$$

$$C'(x)(\pm L) = 0,$$

or

$$\begin{aligned} C''(x) - \frac{\mu_C}{D_C} C(x) &= -\beta\delta(x - x_0) \\ C'(x)(\pm L) &= 0. \end{aligned} \tag{2.13}$$

Let us now consider the linear differentiable operator $LC = C'' - C$.

It turns out that, in order to solve the problem in Equation (2.13), we can instead solve the problem

$$LC = -\frac{\chi K_I}{\epsilon} I(x) = \beta\delta(x - x_0) \tag{2.14}$$

with homogeneous boundary conditions.

Because of the similarity between the behaviours of the δ-function and of our function, we can use the following equation

$$L\left[G(x, x_0)\right] = \delta(x - x_0),$$

where $G(x, x_0)$ is the Green's function.

Thus we see that

$$\beta L\left[G(x,x_0)\right] = LC.$$

Because the operator L is linear, the solution of the problem in Equation (2.13) that we are seeking must have the form

$$C = \beta G. \tag{2.15}$$

In order to find this solution, we will first solve the related problem

$$\begin{gathered} G_{xx}(x;x_0) - \frac{\mu_c}{D_c}G(x;x_0) = -\delta(x-x_0), \quad for \quad x \neq x_0 \\ G_x(\pm L) = 0. \end{gathered} \tag{2.16}$$

The associated characteristic equation is

$$r^2 - \frac{\mu_c C}{D_c},$$

and its roots are

$$r = \pm\sqrt{\frac{\mu_C}{D_C}}.$$

So the solution of problem in Equation (2.16) is

$$G = c_1 e^{\sqrt{\frac{\mu_C}{D_C}}x} + c_2 e^{-\sqrt{\frac{\mu_C}{D_C}}x}.$$

Thus we have that

$$G = A\cosh\left(\sqrt{\frac{\mu_C}{D_C}}x\right) + B\sinh\left(-\sqrt{\frac{\mu_C}{D_C}}x\right).$$

Considering the boundary conditions we obtain

$$G = \begin{cases} A\cosh\left[\sqrt{\frac{\mu_C}{D_C}}(x-L)\right] & 0 < x < L \\ B\cosh\left[\sqrt{\frac{\mu_C}{D_C}}(x+L)\right] & -L < x < 0 \end{cases}$$

Using the symmetry of the solution we can only consider one of the two expressions, namely

$$G = A\cosh\left[\sqrt{\frac{\mu_C}{D_C}}(x-L)\right], \quad \text{when x is near the origin.} \tag{2.17}$$

To determine the constant A we shall use the the following facts about the Green's function on a small interval around the origin $[-\epsilon, \epsilon]$:

$$G(0^+) = G(0^-) \quad \text{(continuity condition)}$$
$$G'(0^+) - G'(0^-) = -1 \quad \text{(jump condition).}$$

Thus we have the system

$$\begin{cases} A\cosh\left[\sqrt{\frac{\mu_C}{D_C}}(x-L)\right] = B\cosh\left[\sqrt{\frac{\mu_C}{D_C}}(x+L)\right] \\ \\ A\sqrt{\frac{\mu_C}{D_C}}\sinh\left[\sqrt{\frac{\mu_C}{D_C}}(x-L)\right] - B\sqrt{\frac{\mu_C}{D_C}}\sinh\left[\sqrt{\frac{\mu_C}{D_C}}(x+L)\right] = -1 \end{cases}$$

with $x \in [-\epsilon, \epsilon]$.

At $x = 0$ this system yields

$$A = -\frac{\cosh\left[\sqrt{\frac{\mu_C}{D_C}}(L)\right]}{\sqrt{\frac{\mu_C}{D_C}}\sinh\left(2\sqrt{\frac{\mu_C}{D_C}}L\right)},$$

which we plug into equation (2.18) to obtain an expression for G:

$$G = -\frac{\cosh\left[\sqrt{\frac{\mu_C}{D_C}}(L)\right]}{\sqrt{\frac{\mu_C}{D_C}}\sinh\left(2\sqrt{\frac{\mu_C}{D_C}}L\right)}\cosh\left[\sqrt{\frac{\mu_C}{D_C}}(x-L)\right].$$

Now we proceed to find the constant β. To this end, we consider the equation on the right side of Equation (2.14), and, after the usual change of variable $x = \epsilon y$, we integrate it over $\mathbb{R}$:

$$\int_{-\infty}^{\infty} -\frac{\chi K_I}{\epsilon}\tilde{I}_0(y)\epsilon\, dy = \int_{-\infty}^{\infty} \beta\delta(x-x_0)\, dx_0,$$
$$\int_{-\infty}^{\infty} -\chi K_I \xi \operatorname{sech}^2\left(y\sqrt{\frac{\xi\chi K_I}{2D_C}}\right)\, dy = \beta\int_{-\infty}^{\infty} \delta(x-x_0)\, dx_0.$$

Thus we obtain

$$-\chi K_I \int_{-\infty}^{\infty} \xi \operatorname{sech}^2\left(y\sqrt{\frac{\xi\chi K_I}{2D_C}}\right)\, dy = \beta,$$

$$\beta = -\chi K_I 2\sqrt{\frac{2D_C\xi}{\chi K_I}} = -2\sqrt{2D_C\xi\chi K_I},$$

where we used the property of the integral of the δ-function over $\mathbb{R}$,

$$\int_{-\infty}^{+\infty} \delta(x-x_0)\, dx_0 = 1.$$

Therefore, plugging our expressions for G and β into Equation (2.15), we have that

$$C = 2\sqrt{2D_C\chi K_I\xi}\frac{\cosh\left[\sqrt{\frac{\mu_C}{D_C}}(L)\right]}{\sqrt{\frac{\mu_C}{D_C}}\sinh\left(2\sqrt{\frac{\mu_C}{D_C}}L\right)}\cosh\left[\sqrt{\frac{\mu_C}{D_C}}(x-L)\right].$$

We may now find the composite solution for C.

In order to do so, we need to consider the behaviour of C near the core of the spike. By integrating the second expression in Equation (2.12) we obtain

$$\widetilde{C}_0 = -2\epsilon\log\left[\cosh\left(y\sqrt{\frac{\xi\chi K_I}{2D_C}}\right)\right],$$

so that in the inner region we have that

$$C \sim \widetilde{C}_0 - 2\epsilon\log\left[\cosh\left(y\sqrt{\frac{\xi\chi K_I}{2D_C}}\right)\right].$$

Using Van Dyke's matching principle, we get the composite solution for C:

$$
\begin{aligned}
C &= C_{\text{inner}} + C_{\text{outer}} - C_{\text{overlap}} \\
&\sim 2\sqrt{2D_C\chi K_I\xi}\frac{\cosh\left[\sqrt{\frac{\mu_C}{D_C}}(L)\right]}{\sqrt{\frac{\mu_C}{D_C}}\sinh\left(2\sqrt{\frac{\mu_C}{D_C}}L\right)}\cosh\left[\sqrt{\frac{\mu_C}{D_C}}(L)\right] \\
&\qquad - 2\epsilon\log\left[\cosh\left(y\sqrt{\frac{\xi\chi K_I}{2D_C}}\right)\right] \\
&\qquad + 2\sqrt{2D_C\chi K_I\xi}\frac{\cosh\left[\sqrt{\frac{\mu_C}{D_C}}(L)\right]}{\sqrt{\frac{\mu_C}{D_C}}\sinh\left(2\sqrt{\frac{\mu_C}{D_C}}L\right)}\cosh\left[\sqrt{\frac{\mu_C}{D_C}}(x-L)\right] \\
&= 2\sqrt{2D_C\chi K_I\xi}\frac{\cosh\left[\sqrt{\frac{\mu_C}{D_C}}(L)\right]}{\sqrt{\frac{\mu_C}{D_C}}\sinh\left(2\sqrt{\frac{\mu_C}{D_C}}L\right)}\left\{\cosh\left(\sqrt{\frac{\mu_C}{D_C}}L\right)+\cosh\left[\sqrt{\frac{\mu_C}{D_C}}(x-L)\right]\right\} \\
&\qquad - 2\epsilon\log\left[\cosh\left(y\sqrt{\frac{\xi\chi K_I}{2D_C}}\right)\right].
\end{aligned}
$$

We now want to find an expression for the height of the spike ξ. In order to do that, we integrate the first equation in Equation (2.4) to obtain the solvability condition:

$$\int_{-L}^{L}\left[\epsilon I_{xx} - (IC_x)_x + \frac{\epsilon^2\alpha_I}{I+\epsilon\beta_I} - \mu_I I\right]dx = 0.$$

Because of the Neumann boundary conditions, $I_x(\pm L,t) = 0 = C_x(\pm L,t)$, we have that

$$\int_{-L}^{L}\epsilon I_{xx}\,dx = 0 \qquad \text{and} \qquad \int_{-L}^{L}(IC_x)_x\,dx = 0.$$

So we have the following integral

$$\int_{-L}^{L}\left(\frac{\epsilon^2\alpha_I}{I+\epsilon\beta_I} - \mu_I I\right)dx = 0,$$

or

$$\int_{-L}^{L}\frac{\epsilon^2\alpha_I}{I+\epsilon\beta_I}\,dx = \int_{-L}^{L}\mu_I I\,dx.$$

Now we use the fact that I is zero almost everywhere in the outer region to obtain

$$\int_{-L}^{L}\frac{\epsilon^2\alpha_I}{I+\epsilon\beta_I}\,dx \sim \int_{-L}^{L}\frac{\epsilon^2\alpha_I}{I+\epsilon\beta_I}\,dx = \frac{2\epsilon\alpha_I L}{\beta_I}$$

and

$$\int_{-L}^{L} \mu_I I \, dx \sim \int_{-\infty}^{\infty} \mu_I \xi \operatorname{sech}^2 \left(y \sqrt{\frac{\xi \chi K_I}{2D_C}} \right) dy = 2\mu_I \sqrt{\frac{2D_C \xi}{\chi K_I}}.$$

Thus we have the equality

$$\frac{2\epsilon \alpha_I L}{\beta_I} = 2\mu_I \sqrt{\frac{2D_C \xi}{\chi K_I}}.$$

Therefore

$$\xi = \frac{\epsilon^2 \alpha_I^2 L^2 \chi K_I}{2D_C \beta_I^2 \mu_I^2}. \tag{2.18}$$

In summary, the uniform asymptotic expansion of Type 1 equilibrium state of (2.3) is given by

$$I \sim \frac{\epsilon^2 \alpha_I^2 L^2 \chi K_I}{2D_C \beta_I^2 \mu_I^2} \operatorname{sech}^2 \left(\frac{x}{\epsilon} \sqrt{\frac{\epsilon^2 \alpha_I^2 L^2 \chi^2 K_I^2}{4D_C^2 \beta_I^2 \mu_I^2}} \right) = \frac{\epsilon^2 \alpha_I^2 L^2 \chi K_I}{2D_C \beta_I^2 \mu_I^2} \operatorname{sech}^2 \left(x \sqrt{\frac{\alpha_I^2 L^2 \chi^2 K_I^2}{4D_C^2 \beta_I^2 \mu_I^2}} \right),$$

$$C \sim 2\sqrt{\frac{\epsilon^2 \alpha_I^2 L^2 \chi^2 K_I^2}{\beta_I^2}} \frac{\cosh\left[\sqrt{\frac{\mu_C}{D_C}}(L)\right]}{\sqrt{\frac{\mu_C}{D_C}} \sinh\left(2\sqrt{\frac{\mu_C}{D_C}} L\right)} \left\{ \cosh\left(\sqrt{\frac{\mu_C}{D_C}} L \right) + \cosh\left[\sqrt{\frac{\mu_C}{D_C}} (x - L) \right] \right\}$$
$$- 2\epsilon \log \left[\cosh \left(\frac{x}{\epsilon} \sqrt{\frac{\xi \chi K_I}{2D_C}} \right) \right].$$

We observe that, since $\xi = O(\epsilon^2)$, the spike is no longer confined to the inner region. This result contradicts the assumption that I behaves like a δ-function. Therefore this Type 1 solution cannot be a solution of our system.

2.3.2 Type 2 Solution

We now examine Type 2 solutions. The spike construction in the inner region $|x| \leq O(\epsilon)$ is identical to the one presented in subsection 2.3.1, and gives rise to the same equations as the ones in Equations (2.12) and (2.18). The difference is that in the outer region I is no longer assumed to be zero, but $O(\epsilon)$. Then the height ξ will

no longer be given by Equation (2.18), but will be determined along with the outer solutions for I and C.

Away from the center of the spike, in the outer region, $|x| > O(\epsilon)$, we scale

$$I = \epsilon \hat{I}.$$

So our Type 2 solution will have the form

$$I = \tilde{I}(y) + \epsilon \hat{I}(x).$$

Here a similar calculation to that in subsection 2.3.1 gives

$$\tilde{I} \sim \xi \operatorname{sech}^2 \left(y \sqrt{\frac{\xi \chi K_I}{2 D_C}} \right)$$

To match the inner and outer regions, we integrate the second equation in Equation (2.4) on a small interval $[0, \delta]$, where $\epsilon << \delta << 1$:

$$\int_0^\delta \left(D_C C_{xx} + \frac{\chi K_I I}{\epsilon} - \mu_C C \right) dx = 0.$$

So we have

$$D_C C_x(\delta) + \frac{\chi K_I}{\epsilon} \int_0^\delta I \, dx = \mu_C \int_0^\delta C \, dx,$$

or

$$C_x(\delta) + \frac{\chi K_I}{\epsilon D_C} \int_0^\delta I \, dx = \frac{\mu_C}{D_C} \int_0^\delta C \, dx. \tag{2.19}$$

We start by considering the term

$$\frac{\chi K_I}{\epsilon D_C} \int_0^\delta I \, dx.$$

In order to estimate the value of this integral, we perform the change of variable $x = \epsilon y$ and obtain

$$\frac{\chi K_I}{\epsilon D_C} \int_0^\delta I \, dx = \frac{\chi K_I}{\epsilon D_C} \int_0^{\frac{\delta}{\epsilon}} \left[\tilde{I}(y) + \epsilon \hat{I}(y) \right] \epsilon \, dy.$$

We notice that, to leading order, we can ignore the term that contains $\epsilon \hat{I}(y)$, so we have

$$\frac{\chi K_I}{\epsilon D_C} \int_0^\delta I \, dx \sim \frac{\chi K_I}{\epsilon D_C} \int_0^{\frac{\delta}{\epsilon}} \tilde{I}(y) \epsilon \, dy.$$

Then we can calculate

$$\begin{aligned}\frac{\chi K_I}{\epsilon D_C}\int_0^{\delta} I\,dx &\sim \frac{\chi K_I}{D_C}\int_0^{\frac{\delta}{\epsilon}} \tilde{I}(y)\,dy \\ &\sim \frac{\chi K_I}{D_C}\int_0^{\infty} \tilde{I}_0\,dy \\ &= \frac{\chi K_I}{D_C}\int_0^{\infty} \xi\,\mathrm{sech}^2\left(y\sqrt{\frac{\xi\chi K_I}{2D_C}}\right)\,dy \\ &= \frac{\xi\chi K_I}{D_C}\sqrt{\frac{2D_C}{\xi\chi K_I}} \\ &= \sqrt{\frac{2\xi\chi K_I}{D_C}}.\end{aligned}$$

We also have that

$$\int_0^{\delta} C\,dx = \frac{2}{\epsilon}\sqrt{2D_C\chi K_I\xi}\frac{\cosh\left[\sqrt{\frac{\mu_C}{D_C}}(L)\right]}{\sqrt{\frac{\mu_C}{D_C}}\sinh\left(2\sqrt{\frac{\mu_C}{D_C}}L\right)}\int_0^{\delta}\cosh\left[\sqrt{\frac{\mu_C}{D_C}}(x-L)\right]\,dx.$$

Since, as $\delta \to 0$,

$$\int_0^{\delta}\cosh\left[\sqrt{\frac{\mu_C}{D_C}}(x-L)\right] = \frac{\sinh\left(\sqrt{\frac{\mu_C}{D_C}}L\right)}{\sqrt{\frac{\mu_C}{D_C}}} - \frac{\sinh\left(\sqrt{\frac{\mu_C}{D_C}}L - \frac{\mu_C}{D_C}\delta\right)}{\sqrt{\frac{\mu_C}{D_C}}} \to 0,$$

we have $\int_0^{\delta} C\,dx = O(\delta)$.

Substituting these into Equation 2.19, we obtain the following expression:

$$C_x(\delta) = -\frac{\chi K_I}{\epsilon D_C}\int_0^{\delta} I dx + \frac{\mu_C}{D_C}\int_0^{\delta} C dx = -\sqrt{\frac{2\xi\chi K_I}{D_C}} + \frac{\mu_C}{D_C}O(\delta).$$

Therefore, to leading order, in the outer region we have that

$$C'(0^+) \sim -\sqrt{\frac{2\xi\chi K_I}{D_C}}. \tag{2.20}$$

We now want to find C in the outer region. In order to do that, we look at the equilibrium system

$$\begin{aligned} \epsilon^2 \hat{I}_{xx} - \epsilon(\hat{I}C_x)_x + \frac{\epsilon\alpha_I}{\hat{I}+\beta_I} - \epsilon\mu_I\hat{I} = 0 \\ D_c C_{xx} + \chi K_I \hat{I} - \mu_C C = 0. \end{aligned} \tag{2.21}$$

Since $\epsilon << 1$, to leading order, the steady state satisfies the system

$$\begin{aligned} (\hat{I}C_x)_x - \frac{\alpha_I}{\hat{I}+\beta_I} + \mu_I\hat{I} = 0 \\ D_c C_{xx} + \chi K_I \hat{I} - \mu_C C = 0. \end{aligned} \tag{2.22}$$

In order to find our solution, we would like each equation of this system to involve solely the I function and its derivatives or solely the C function and its derivatives. But, since $I \neq 0$ in the outer region, the variables I and C are still linked; i.e., the system is still coupled.

To decouple this system, we proceed as follows.

From the first equation in Equation (2.22) we get

$$(\hat{I}C_x)_x(\hat{I}+\beta_I) + \mu_I\hat{I}(\hat{I}+\beta_I) - \alpha_I = 0,$$

$$(\hat{I}_x C_x + \hat{I}C_{xx})(\hat{I}+\beta_I) + \mu_I\hat{I}(\hat{I}+\beta_I) - \alpha_I = 0,$$

$$(\hat{I}C_x)_x = \hat{I}_x C_x + \hat{I}C_{xx} = \frac{\alpha_I - \mu_I\hat{I}^2 - \beta_I\mu_I\hat{I}}{\hat{I}+\beta_I},$$

$$\hat{I}\hat{I}_x C_x + \beta_I\hat{I}_x C_x + \hat{I}^2 C_{xx} + \beta_I\hat{I}C_{xx} + \mu_I\hat{I}^2 + \beta_I\mu_I\hat{I} - \alpha_I = 0.$$

Solving for $\hat{I} = \frac{\mu_C C - D_C C''}{\chi K_I}$, which we get from the second equation in Equation (2.22), we obtain a third order ordinary differential equation (ODE) for C in the outer region:

$$
\begin{aligned}
0 &= \frac{1}{\chi^2 K_I^2}(\mu_C C - D_C C'')(\mu_C C - D_C C'')' C' + \frac{1}{\chi K_I}\beta_I(\mu_C C - D_C C'')' C' \\
&\quad + \frac{1}{\chi^2 K_I^2}\mu_I(\mu_C C - D_C C'')^2 + \frac{1}{\chi K_I}\beta_I\mu_I(\mu_C C - D_C C'') \\
&\quad + \frac{1}{\chi^2 K_I^2}(\mu_C C - D_C C'')^2 C'' + \frac{1}{\chi K_I}\beta_I(\mu_C C - D_C C'')C'' - \alpha_I \\
&= (\mu_C C - D_C C'')(\mu_C C' - D_C C''')C' + \beta_I \chi K_I(\mu_C C' - D_C C''')C' \\
&\quad + \mu_I(\mu_C C - D_C C'')^2 + \beta_I\mu_I\chi K_I(\mu_C C - D_C C'') \\
&\quad + (\mu_C C - D_C C'')^2 C'' + \beta_I\chi K_I(\mu_C C - D_C C'')C'' - \alpha_I\chi^2 K_I^2 \\
&= (\mu_C C - D_C C'')[(\mu_C C' - D_C C''')C' + \mu_I(\mu_C C - D_C C'')(\mu_C C - D_C C'')C''] \\
&\quad + \beta_I\chi K_I[(\mu_C C' - D_C C''')C' + \mu_I(\mu_C C - D_C C'') + (\mu_C C - D_C C'')C''] \\
&\quad - \alpha_I\chi^2 K_I^2.
\end{aligned}
$$

So

$$
\begin{aligned}
0 &= (\mu_C C - D_C C'' + \beta_I\chi K_I)[C'(\mu_C C' - D_C C''') + C''(\mu_C C - D_C C'') \\
&\quad + \mu_I(\mu_C C - D_C C'')] - \alpha_I\chi^2 K_I^2.
\end{aligned}
$$

We shall now proceed to find the appropriate boundary conditions for this ODE.

We obtain the first one directly from the Neumann boundary conditions (see Equation (2.2)) , namely

$$C'(L) = 0.$$

We can also obtain the second boundary condition directly from Equation (2.20), namely

$$C'(0) \sim -\sqrt{\frac{2\xi\chi K_I}{D_C}}.$$

In order to find the third boundary condition, we substitute the expression $\hat{I} = \frac{\mu_C C - D_C C''}{\chi K_I}$ into the equation

$$\hat{I}C_x - \frac{\alpha_I}{\hat{I} + \beta_I} + \mu_I\hat{I} = 0,$$

which we have obtained by applying the Neumann boundary conditions to the first equation in Equation (2.21).

Therefore we get

$$\begin{aligned}
0 &= \frac{\mu_C C - D_C C_{xx}}{\chi K_I} C_{xx} - \frac{\alpha_I}{\frac{\mu_C C - D_C C_{xx}}{\chi K_I} + \beta_I} + \frac{\mu_C C - D_C C_{xx}}{\chi K_I} \mu_I \\
&= \frac{(\mu_C C - D_C C_{xx})\, C_{xx} + \mu_I\, (\mu_C C - D_C C_{xx})}{\chi K_I} - \frac{\alpha_I \chi K_I}{(\mu_C C - D_C C_{xx}) + \beta_I \chi K_I} \\
&= (\mu_C C - D_C C_{xx})\, C_{xx}\, [(\mu_C C - D_C C_{xx}) + \beta_I \chi K_I] \\
&\qquad + \mu_I\, (\mu_C C - D_C C_{xx})\, [(\mu_C C - D_C C_{xx}) + \beta_I \chi K_I] - \alpha_I (\chi K_I)^2 \\
&= D_C^2 (C_{xx})^3 + \left(D_C^2 \mu_I - 2 D_C \mu_C C - \beta_I \chi K_I D_C\right) (C_{xx})^2 \\
&\qquad + \left(\mu_C^2 C^2 + \beta_I \chi K_I C - 2 D_C \mu_C \mu_I C - \beta_I \chi K_I D_C \mu_I\right) C_{xx} \\
&\qquad + \mu_C^2 \mu_I C^2 + \beta_I \chi K_I \mu_C \mu_I C - \alpha_I (\chi K_I)^2
\end{aligned}$$

Using Maple™ (see Appendix for the Maple™ worksheet) we find the three roots – one real and two complex – of this cubic equation. We can use the real root as the third boundary condition we seek; for our convenience we will denote it by $rr1$, similarly to worksheet.

In summary, in order to find C in the outer region, we have to solve the third order ODE

$$\begin{aligned}
0 = (\mu_C C - D_C C'' + \beta_I \chi K_I)[C'(\mu_C C' - D_C C''') + C''(\mu_C C - D_C C'') \\
+ \mu_I (\mu_C C - D_C C'')] - \alpha_I \chi^2 K_I^2
\end{aligned}$$

subject to the boundary conditions

$$C'(L) = 0; \quad C'(0) \sim -\sqrt{\frac{2\xi \chi K_I}{D_C}}; \quad C''(L) = rr1.$$

This is a third order nonlinear problem whose exact solution might be very hard to find, if even possible. We shall then seek an approximate solution C. Luckily Maple™solver shall come to our aid, in that we will use the Continuation Method first

and then the Newton's Method for systems – which are included into the software – to find a numerical solution C for different values of ξ.

Note that those values of the function C are not shown explicitly, but are used in subsequent calculations to find the height of the spike at the origin (see Appendix).

The next step towards calculating ξ requires us to integrate the first equation in Equation (2.4) on the interval $[-L, L]$:

$$\int_{-L}^{L} \left[\epsilon I_{xx} - (IC_x)_x + \frac{\epsilon^2 \alpha_I}{I + \epsilon\beta_I} - \mu_I I \right] dx = 0.$$

Because of the boundary conditions, we have that

$$\int_{-L}^{L} \epsilon I_{xx} dx = 0 \quad \text{and} \quad \int_{-L}^{L} (IC_x)_x dx = 0.$$

Thus we are left with the following integral:

$$\int_{-L}^{L} \left(\frac{\epsilon^2 \alpha_I}{I + \epsilon\beta_I} - \mu_I I \right) dx = 0,$$

or

$$\int_{-L}^{L} \frac{\epsilon^2 \alpha_I}{I + \epsilon\beta_I} dx = \int_{-L}^{L} \mu_I I dx.$$

Since we look for a solution of the form $I = \tilde{I}(y) + \epsilon\hat{I}(x)$, we can re-write our integral in the following way:

$$\int_{-L}^{L} \frac{\epsilon^2 \alpha_I}{\frac{1}{\epsilon}\left(\tilde{I}\left(\frac{x}{\epsilon}\right) + \epsilon\hat{I}\right) + \epsilon\beta_I} dx = \int_{-L}^{L} \epsilon\mu_I \hat{I} dx + \int_{\frac{-L}{\epsilon}}^{\frac{L}{\epsilon}} \epsilon \frac{1}{\epsilon} \mu_I I \left(\frac{x}{\epsilon}\right) dx.$$

We know from our simulation that the contribution of $I(\frac{x}{\epsilon})$ in the expression on the left-hand side is negligible. We will then omit this quantity from the calculations. The same is not true in the expression on the right-hand side.

So we can re-write our equation as

$$\int_{-L}^{L} \frac{\epsilon^2 \alpha_I}{\epsilon\hat{I} + \epsilon\beta_I} dx = \int_{-L}^{L} \epsilon\mu_I \hat{I} dx + \int_{\frac{-L}{\epsilon}}^{\frac{L}{\epsilon}} \epsilon \frac{1}{\epsilon} \mu_I I \left(\frac{x}{\epsilon}\right) dx.$$

After we have performed the change of variable $x = \epsilon y$ and simplified, we obtain

$$\int_{-L}^{L} \frac{\epsilon\alpha_I}{\hat{I} + \beta_I} dx = \epsilon\mu_I \int_{-L}^{L} \hat{I} dx + \epsilon\mu_I \int_{-\infty}^{\infty} \tilde{I}(y) dy,$$

or

$$\int_{-L}^{L} \frac{\alpha_I}{\hat{I}+\beta_I} dx = \mu_I \int_{-L}^{L} \hat{I} dx + \mu_I \int_{-\infty}^{\infty} \tilde{I}(y) dy,$$

hence

$$\int_{-L}^{L} \left(\frac{\alpha_I}{\hat{I}+\beta_I} - \mu_I \hat{I} \right) dx = \mu_I \int_{-\infty}^{\infty} \tilde{I}(y)\, dy.$$

From our calculation for the Type 1 solution, we know that

$$\int_{-\infty}^{\infty} \tilde{I}(y)\, dy \sim \int_{-\infty}^{\infty} \xi \operatorname{sech}^2 \left(y \sqrt{\frac{\xi \chi K_I}{2D_C}} \right) dy = 2\sqrt{\frac{2D_C \xi}{\chi K_I}};$$

thus

$$\int_{-L}^{L} \left(\frac{\alpha_I}{\hat{I}+\beta_I} - \mu_I \hat{I} \right) dx \sim 2\mu_I \sqrt{\frac{2D_C \xi}{\chi K_I}}. \tag{2.23}$$

We now recall that we found numerical approximations of C for different values of ξ. If we were to plug those values into the equation $\hat{I} = \frac{\mu_C C - D_C C''}{\chi K_I}$, we would obtain numerical approximations of $\hat{I}$ at different ξs, $\hat{I}(C;\xi)$. This means that we can find the values of the integral on the left-hand side in Equation (2.23) for given values of ξ. Hence we can treat the said integral as a function of ξ:

$$f_1(\xi) \sim \int_{-L}^{L} \left(\frac{\alpha_I}{\hat{I}+\beta_I} - \mu_I \hat{I} \right) dx.$$

It is clear that we can also treat the right-hand side of equation (2.23) as a function of ξ:

$$f_2(\xi) \sim 2\mu_I \sqrt{\frac{2D_C \xi}{\chi K_I}}.$$

By resorting to Maple™ again, we can plot $f_1(\xi)$ and $f_2(\xi)$ and find the value of ξ we are looking for at the point where the functions intersect; we will denote this value by ξ^*. Indeed, we have found that $\xi^* = 1.840230049$ (see Appendix).

We can now use this value ξ^* to obtain the solution I that we seek.

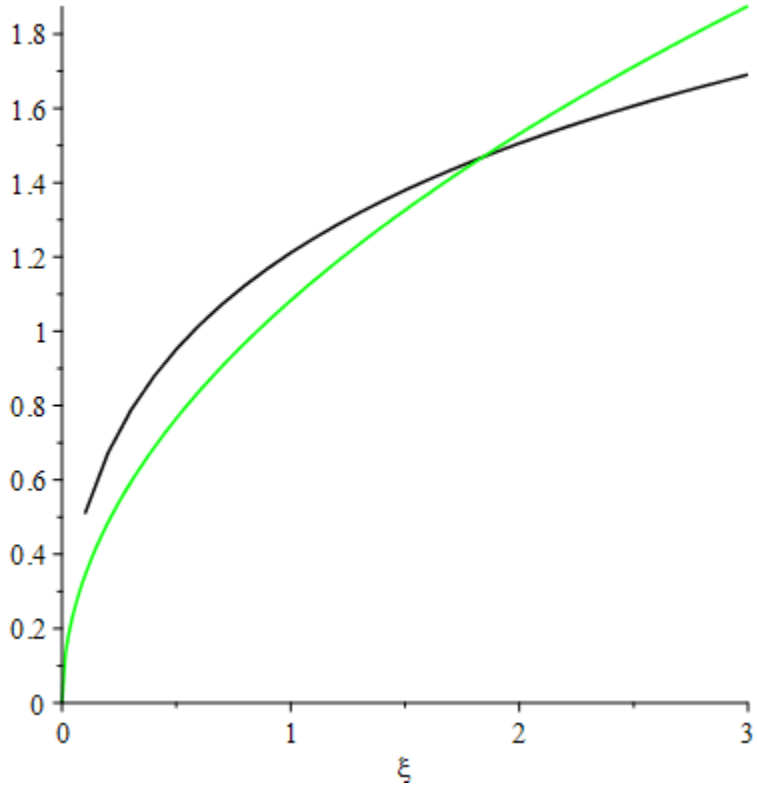

Figure 2.1: Graphs of $f_1(\xi)$ (black) and $f_2(\xi)$ (green).

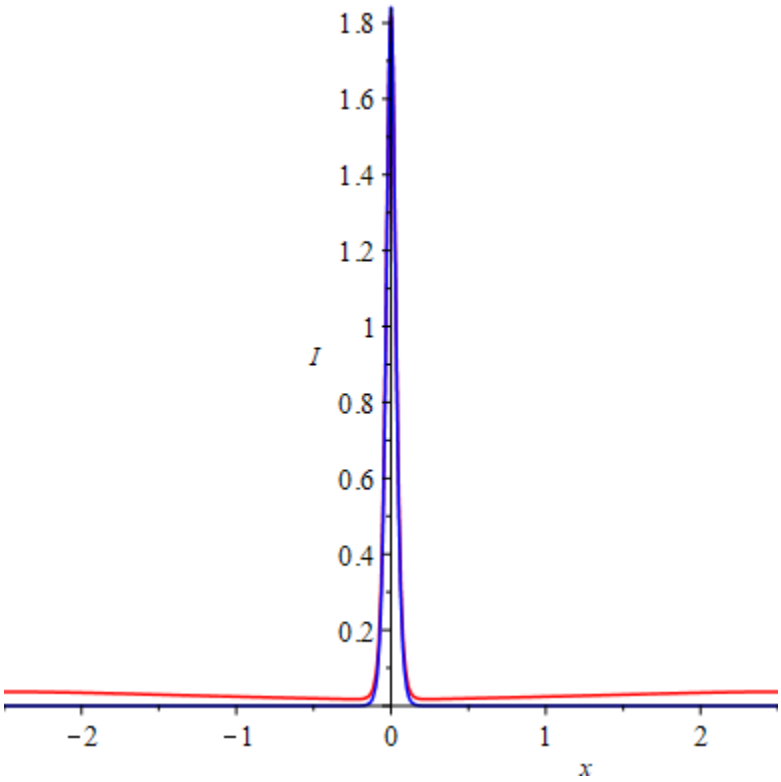

Figure 2.2: Graphs of I (the equilibrium density of immune cells) in the inner region, obtained by using Maple™ (blue) and FlexPDE (red). The calculations were performed using the following parameters: $\epsilon = 0.1$, $\alpha_I = 0.75$, $\beta_I = 1$, $\mu_I = 1$, $D_C = 4$ $K_I = 1.95$, $\chi = 14$, $\mu_C = 4$.

Therefore we have obtained the following solution:

$$I \sim \xi^* \operatorname{sech}^2\left(\frac{x}{\epsilon}\sqrt{\frac{\xi^*\chi K_I}{2D_C}}\right) + \epsilon\frac{\mu_C C - D_C C''}{\chi K_I} \quad \text{and} \quad C = f(x;t).$$

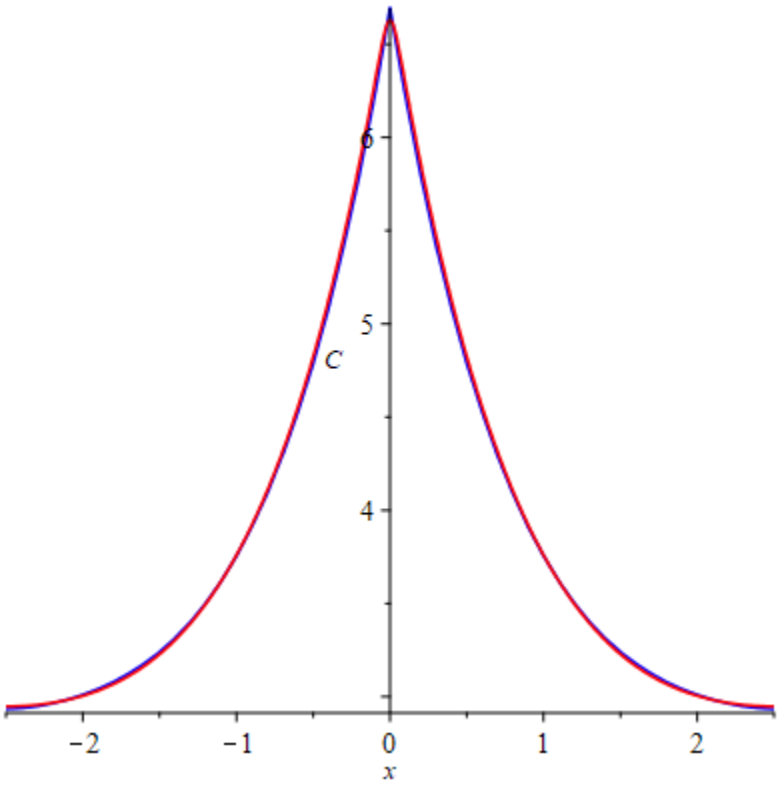

Figure 2.3: Graphs of C (the equilibrium concentration of chemoattractant) obtained by using Maple™ (blue) and FlexPDE (red). The calculations were performed using the following parameters: $\epsilon = 0.1$, $\alpha_I = 0.75$, $\beta_I = 1$, $\mu_I = 1$, $D_C = 4$ $K_I = 1.95$, $\chi = 14$, $\mu_C = 4$.

Chapter 3

Conclusion

In this work we have proposed a mathematical model of the inflammatory response involved in the formation of an atherosclerotic plaque. Our focus has been on the early stages of this process, specifically on the immune system response to chemical stimuli secreted by endothelial cells, monocytes/macrophages, and other cells after injury to the arterial wall and lipid accumulation in the intimal layer. This response is characterized by chemotaxis, which consists of the movement of immune cells from the arterial blood to the site of plaque formation, in the intima. We studied it by using suitable mathematical techniques. The foremost mathematical model that describes chemotaxis is the Keller-Segel model, first presented in 1970 [18]. The "classical" Keller-Segel model corresponds to setting $\alpha_I = 0$ and $\mu_I = 0$ in the first equation in Equation (2.1).

The question that we wanted to answer in this paper was whether our model could generate a pattern, that is, describe aggregation, or, in our case describe atherosclerotic plaque formation. In order to give a positive answer, we needed to find solutions of our system of PDEs that are stable, i.e., that neither collapse to a point (chemotactic collapse) nor grow without bound (blow-up solution), and whose spike dynamics are consistent with a self-sustained process.

Our study of the basic pattern formation yielded two types of spike solutions that we called Type 1 and Type 2. Notice that in both cases we focused on the study of a single spike. The behaviour of the solutions and their stability has been partly inferred from numerical simulations and partly shown analytically by our calculations.

Our results strongly suggest that Type 1 solution is not a viable solution of the reaction-diffusion system introduced in our model, since its existence would contradict our working assumptions. On the other hand, Type 2 solution can be accepted as a

solution of the system, in that it does not vanish as $x \to \pm\infty$, is stable, and it does not blow up in a finite time. Hence, our results suggest that, under the appropriate conditions, our model does generate a pattern; thus, our model can describe the early stages of atherosclerotic plaque formation.

We acknowledge that we have imposed a number of simplifications in this study that are not fully consistent with the complex nature of atherogenesis — e.g., taking fixed boundaries, ignoring HDL cholesterol, assuming a constant level of free radicals and so on. This allows us to capture some of the characteristics of the disease but not others.

Our intent is not to propose that the system is a definitive model of atherogenesis, but rather to offer a preliminary mathematical framework with which we begin to study the onset of atherosclerosis as the result of chronic inflammation.

It must be stressed that our work was intended to be a viability study of the mathematical model we had built. Therefore our results are to be considered preliminary; nonetheless they are encouraging and seem to warrant further investigations. These should include a full stability analysis of our solutions and a study of the spike dynamics.

The present work could be enriched in several ways. For instance, since atherosclerotic plaques seem to form preferentially near branch points and along inner curvatures, where the endothelial shear stress is low or oscillatory, it would be interesting to include in a future model the changes in the blood flow along the arteries. Another interesting addition would be that of an advection term of the form $-u_x I_x$ in the first equation of Equation (2.2). This term represents the contribution of the blood flow with velocity u_x to the change in the concentration of the immune cells present in the region considered in the model. Numerical simulations showed that our system has a very interesting dymanics with spike creation, spike insertion, and periodic behaviour (see Figure 3.1). So it would be worthwhile to do an analysis of these regimes. It would also be desirable to test our model in two and three dimensions.

We also want to mention that a future cooperation with experts in biomechanics,

biophysics, biochemistry, and medicine could be beneficial, in particular to set up experiments providing appropriate data.

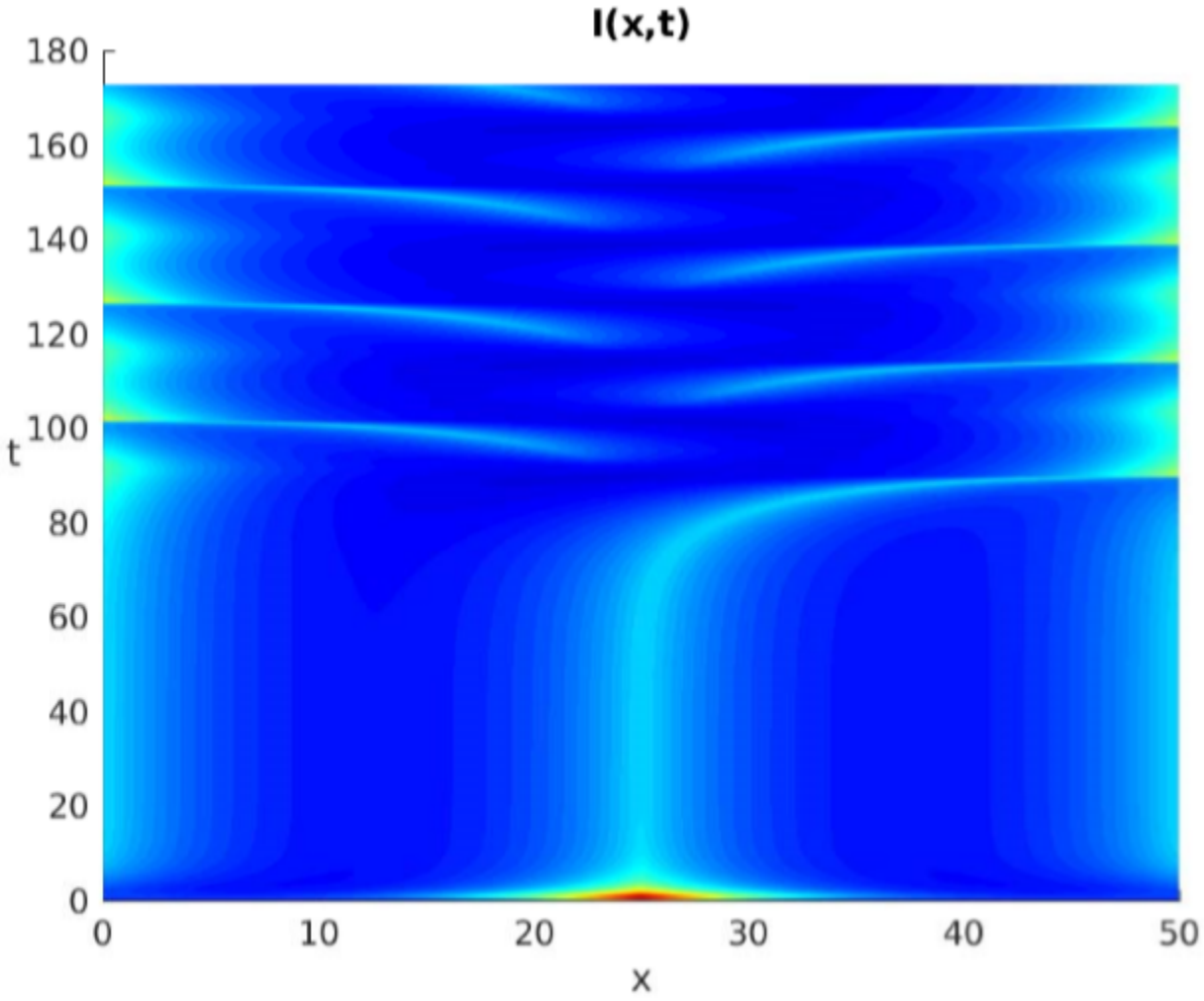

Figure 3.1: This figure shows an example of the dynamics that can be generated by the system in Equation (2.3). In particular here it is shown a periodic dynamics of the contour plot of I in time and space, where spikes are formed in the middle of the region in the picture, and then migrate to its boundaries. The picture was obtained using MATLAB® R2018b © 1984-2018 The Mathworks, Inc. The calculations were performed using the following parameters: $\epsilon = 0.1$, $\alpha_I = 0.75$, $\beta_I = 1$, $\mu_I = 1$, $D_C = 2$ $K_I = 1.95$, $\chi = 14$, $\mu_C = 4$.

Bibliography

[1] Burden, R. L. and Faires, J. D., *Numerical analysis*, Brooks/Cole Pub. Co, 2005.

[2] Calvez, V., Houot, J. G., Meunier, N., Raoult, A., and Rusnakova, G., *Mathematical and numerical modeling of early atherosclerotic lesions*, ESAIM: Proceedings (2010).

[3] Caro, C. G. and Fitz-Gerald, J. M., Schroter R. C., Lighthill, M. J., and Parke Stoker, M. G., *Atheroma and arterial wall shear - observation, correlation and proposal of a shear dependent mass transfer mechanism for atherogenesis*, Proceedings of the Royal Society of London. Series B. Biological Sciences **177** (1971), no. 1046, 109–133.

[4] Chalmers, A. D. and Cohen, A. and Bursill, C. A. and Myerscough, M. R., *Bifurcation and dynamics in a mathematical model of early atherosclerosis*, Journal of Mathematical Biology **71** (2015), no. 6, 1451–1480.

[5] Cobbold, C. A., Sherratt, J. A., and Maxwell, S. R J, *Lipoprotein oxidation and its significance for atherosclerosis: A mathematical approach*, Bulletin of Mathematical Biology (2002).

[6] de Korte, C. L. and van der Steen, A.F.W., *Intravascular ultrasound elastography: an overview*, Ultrasonics **40** (2002), no. 1, 859 – 865.

[7] El Khatib, N. , Genieys, S., Kazmierczak, B., and Volpert, V., *Reaction–diffusion model of atherosclerosis development*, Journal of Mathematical Biology **65** (2012), no. 2, 349–374.

[8] El Khatib, N., Génieys, S., and Volpert, V., *Atherosclerosis initiation modeled as an inflammatory process*, Math. Model. Nat. Phenom. **2** (2007), no. 2, 126–141.

[9] Fan, J. and Watanabe, T., *Inflammatory reactions in the pathogenesis of atherosclerosis*, Journal of Atherosclerosis and Thrombosis **10** (2003), no. 2, 63–71.

[10] Haberman, R., *Applied partial differential equations: With fourier series and boundary value problems.*, Pearson Prentice Hall., 2004.

[11] G. K. Hansson, *Inflammation, atherosclerosis, and coronary artery disease*, New England Journal of Medicine **352** (2005), no. 16, 1685–1695, PMID: 15843671.

[12] Hansson, G. K. and Libby, P., *Hansson gk, libby pthe immune response in atherosclerosis: a double-edged sword. nat rev immunol 6:508-519*, Nature reviews. Immunology **6** (2006), 508–19.

[13] Hidalgo, A., Tello, L., and Toro, E. F., *Numerical and analytical study of an atherosclerosis inflammatory disease model*, Journal of Mathematical Biology **68** (2014), no. 7, 1785–1814.

[14] Holzapfel, G., Gasser, T., and Ogden, R.W., *A new constitutive framework for arterial wall mechanics and a comparative study of material models*, Journal of Elasticity **61** (2000).

[15] Horstmann, D., *From 1970 until present: The keller-segel model in chemotaxis and its consequences ii*, Jahresbericht der DMV **106** (2004), 51–69.

[16] Humphrey, J.D., *Cardiovascular solid mechanics: Cells, tissues, and organs*, vol. 55, 01 2002.

[17] Ibragimov, A. I., McNeal, C. J., Ritter, L. R., and Walton, J. R., *A mathematical model of atherogenesis as an inflammatory response*, Mathematical Medicine and Biology: A Journal of the IMA (2005).

[18] Keller, E. F. and Segel, L. A., *Initiation of slime mold aggregation viewed as an instability*, Journal of Theoretical Biology **26** (1970), no. 3, 399 – 415.

[19] ———, *Model for chemotaxis*, Journal of Theoretical Biology **30** (1971), no. 2, 225 – 234.

[20] Kolokolnikov, T., Wei, J., and Alcolado, A., *Basic mechanisms driving complex spike dynamics in a chemotaxis model with logistic growth*, SIAM Journal of Applied Mathematics (2014).

[21] Li, Z. -Y., Howarth, S. P.S., Tang, T., and Gillard, J. H., *How critical is fibrous cap thickness to carotid plaque stability?*, Stroke (2006).

[22] Libby, P., *Inflammation in atherosclerosis*, Arteriosclerosis, Thrombosis, and Vascular Biology **32** (2019), no. 9, 2045–2051.

[23] Libby, P. and Ridker, P. M., *Inflammation and atherothrombosis: From population biology and bench research to clinical practice*, Journal of the American College of Cardiology **48** (2006), no. 9, Supplement, A33 – A46, Critical Issues in Cardiovascular Research.

[24] Libby, P., Ridker, P. M., and Maseri, A., *Inflammation and atherosclerosis*, Circulation (2002).

[25] Lutgens, E., de Muinck, E. D., Kitslaar, P. J.E.H.M., Tordoir, J. H.M., Wellens, H. J.J., and Daemen, M. J.A.P., *Biphasic pattern of cell turnover characterizes the progression from fatty streaks to ruptured human atherosclerotic plaques*, Cardiovascular Research (1999).

[26] Neumann, S. J., Berceli, S. A., Sevick, E. M., Lincoff, A. M., Warty, V. S., Brant, A. M., Herman, I. M., and Borovetz, H. S., *Experimental determination and mathematical model of the transient incorporation of cholesterol in the arterial wall*, Bulletin of Mathematical Biology **52** (1990), no. 6, 711–732.

[27] Ougrinovskaia, A., Thompson, R. S., and Myerscough, M. R., *An ode model of early stages of atherosclerosis: Mechanisms of the inflammatory response*, Bulletin of Mathematical Biology **72** (2010), no. 6, 1534–1561.

[28] Ross, R.., *The pathogenesis of atherosclerosis: a perspective for the 1990s*, Nature (1993).

[29] Ross, R., *Atherosclerosis — an inflammatory disease*, New England Journal of Medicine **340** (1999), no. 2, 115–126, PMID: 9887164.

[30] Saidel, G. M., Morris, E. D., and Chisolm, G. M., *Transport of macromolecules in arterial wallin vivo: A mathematical model and analytical solutions*, Bulletin of Mathematical Biology **49** (1987), no. 2, 153–169.

[31] Tang ,D., Yang, C., Kobayashi S., Zheng, J., Woodard, P.K., Teng, Z., Billiar, K., Bach, R., and Ku, D.N., *3d mri-based anisotropic fsi models with cyclic bending for human coronary atherosclerotic plaque mechanical analysis.*, J Biomech Eng. (2009).

[32] Tang, D., Yang, C., Zheng, J., Woodard, P. K., Sicard, G. A., Saffitz, J. E., and Yuan, C., *3d mri-based multicomponent fsi models for atherosclerotic plaques*, Annals of Biomedical Engineering **32** (2004), no. 7, 947–960.

[33] Wentzel, J. J., Chatzizisis, Y. S., Gijsen, F. J.H., Giannoglou, G. D., Feldman, C. L., and Stone, P. H., *Endothelial shear stress in the evolution of coronary atherosclerotic plaque and vascular remodelling: current understanding and remaining questions*, Cardiovascular Research (2012).

[34] Wikipedia contributors, *Artery — Wikipedia, the free encyclopedia*, 2019, [Online; accessed 18-June-2019].

[35] Yang, Y. and Jäger, W., Neuss-Radu, M., and Richter, T., *Mathematical modeling and simulation of the evolution of plaques in blood vessels*, Journal of Mathematical Biology **72** (2016), no. 4, 973–996.